Spectral and Textural Features for Predicting Soil Phosphorus Using Vis-NIR Point Data and Multispectral UAV Imagery: A Case Study From a Long-Term Experiment

Article *in* Journal of Plant Nutrition and Soil Science · June 2025

DOI: 10.1002/jpln.12012

7 authors, including:

Yousra El-Mejjaouy
University of Bern
7 PUBLICATIONS **20** CITATIONS
SEE PROFILE

Jeroen Meersmans
University of Liège
129 PUBLICATIONS **7,780** CITATIONS
SEE PROFILE

Abdallah Oukarroum
Mohammed VI Polytechnic University
152 PUBLICATIONS **7,780** CITATIONS
SEE PROFILE

Journal of Plant Nutrition and Soil Science

WILEY-VCH

RESEARCH ARTICLE

Spectral and Textural Features for Predicting Soil Phosphorus Using Vis-NIR Point Data and Multispectral UAV Imagery: A Case Study From a Long-Term Experiment

Yousra El-Mejjaouy[1,2] | Jean-François Bastin[3] | Vincent Baeten[4] | Jeroen Meersmans[5] | Abdallah Oukarroum[3] | Benjamin Dumont[6] | Benoît Mercatoris[1]

[1]Gembloux Agro-Bio Tech, Biosystems Dynamics and Exchanges, TERRA Teaching and Research Centre, University of Liege, Gembloux, Belgium | [2]Plant Stress Physiology Laboratory, University Mohammed VI Polytechnic (UM6P)—AgroBioSciences, Benguerir, Morocco | [3]Gembloux Agro-Bio Tech, Biodiversity and Landscape Unit, University of Liege, Gembloux, Belgium | [4]Valorisation of Agricultural Products Department, Walloon Agricultural Research Centre (CRA-W), Gembloux, Belgium | [5]TERRA Teaching and Research Centre, Gembloux Agro-Bio Tech, University of Liège, Gembloux, Belgium | [6]Gembloux Agro-Bio Tech, Pant Sciences/Crop Science, TERRA Teaching and Research Centre, University of Liege, Gembloux, Belgium

Correspondence: Yousra El-Mejjaouy (Yousra.el-mejjaouy@uliege.be) | Benoît Mercatoris (benoit.mercatoris@uliege.be)

Received: 28 April 2024 | **Revised:** 18 March 2025 | **Accepted:** 16 April 2025

Academic Editor: Scholten Thomas

Funding: Financial support was provided by OCP Group and Prayon.

Keywords: multispectral imaging | soil phosphorus | texture features | unmanned aerial vehicle | vegetation indices | visible and near-infrared spectroscopy

ABSTRACT

Soil nutrient status assessment is a key aspect of crop management. Unlike the labor- and time-intensive conventional approach, precision farming techniques are expanding to ensure the uniformity of soil nutrients, enhance production, and alleviate economic pressure.

Aims: In this study, the potentials of visible and near-infrared spectroscopy (Vis-NIRS), as non-imaging technology and multispectral imagery mounted on unmanned aerial vehicle (UAV) to predict plant-available (AP) and total phosphorus (TP) (P) were studied and compared.

Materials & Methods: Soil samples were taken from a long-term experiment with contrasting fertilization treatments, and their spectra were recorded. Additionally, drone multispectral images were taken before and after soil tillage and seedbed preparation.

Results: The predicted available P content by Vis-NIRS was characterized by a cross-validation determination coefficient of $R^2_{cv} = 0.82$ and validation determination coefficient of $R^2_{v} = 0.74$, whereas the root mean square error for cross-validation ($RMSE_{cv}$) and validation ($RMSE_{v}$) were, respectively, 11.23 and 14.09 mg kg^{-1}. The random forest (RF) model based on the textural and spectral features from multispectral images taken after seedbed preparation had the highest performances to predict plant-available P ($R^2_{v} = 0.68$, $RMSE_{v} = 13.65$ mg kg^{-1}, and $RPIQ_{v} = 2.98$), whereas the lowest prediction accuracy was obtained for total P prediction model after seedbed preparation ($R^2_{v} = 0.40$, $RMSE_{v} = 67.91$, and $RPIQ_{v} = 0.6$). The effective wavelengths were around 450, 580, and 700 nm for predicting the available P fraction. Before soil tillage, the vegetation indices ranked high in the RF prediction models for available phosphorus (AP) and TP as compared to those developed after using tillage image-derived indices. In contrast, red-

Benjamin Dumont and Benoît Mercatoris share senior co-authorship on this article.

edge, red, and green bands, in addition to texture indices, were the most important predictors of soil available P following seedbed preparation.

Conclusion: Our study suggests that soil tillage and seedbed preparation incorporate vegetation cover and alter soil roughness, resulting in a more homogeneous, smoother surface and higher accuracy for soil P prediction using UAV multispectral imagery.

1 | Introduction

Soil fertilization is a crucial part of crop management to meet plants' nutrient requirements. The determination of the amount, type, and timing of the applied fertilizer depends on the soil's nutrient content in addition to a wide range of factors related to agro-management decisions, such as crop type and the fertilizer form, as well as weather conditions (Madsen 1995). The soil's nutrient content is usually quantified using a conventional analysis in the laboratory, which is labor-intensive, costly, and time-consuming. Hence, typically only a restricted amount of soil samples can be considered which does not allow exploring spatial distribution at the desired level of detail (e.g., detecting the within-field variability), especially when developing precision farming to support sustainable agro-management across larger geographical entities (e.g., at the field, farm, or catchment scale). From small scale to large scale, soil chemical and physical characteristics can differ strongly, particularly phosphorus as it has a rather high spatial variability within agro-ecosystems. The parent material, the biota present, climate variables, and soil biogeochemical processes are the key factors affecting its distribution (Stewart and Tiessen 1987; J. Zhu et al. 2021). Thus, it is important to develop phosphorus content estimation techniques to gather soil content information quickly and affordably over large areas.

Proximal and remote sensing techniques have gained attention as noninvasive tools for estimating crop and soil properties. Most optical spectroscopy and imaging studies on soil properties sensing have focused on texture, organic matter, and clay mineralogy due to their direct spectral response in the visible near-infrared spectra (Kuang et al. 2012). Soil phosphorus in addition to other soil nutrients has an indirect spectral response because it is dependent on a combination of other soil properties (Kodaira and Shibusawa 2013). The relationship between phosphorus content and soil spectral features has been extensively investigated (Bogrekci and Lee 2006). Nevertheless, the results were often highly variable and typically characterized by moderate performance. In the determination of plant-available phosphorus (AP) using visible and near-infrared spectroscopy (Vis-NIRS), coefficients of determination (R^2) superior to 0.7 were reported by different authors (Maleki et al. 2007; Abdi et al. 2016; Kawamura et al. 2019; Pätzold et al. 2019), whereas other studies reported fairly poor predictions with models' R^2 values inferior to 0.7 (Hu et al. 2016; Wijewardane et al. 2018). Zhang et al. (2017) attributed the poor soil phosphorus prediction to its weak correlation with fundamental soil properties with well-defined features. The well-known absorption features in the Vis-NIR near 1400 and 1900 nm are primarily caused by O–H bonds and water; clay minerals cause absorptions in the vicinity of 2200 nm (Viscarra Rossel et al. 2016). Gholizadeh et al. (2013) found a significant positive correlation between phosphorus and bands of absorption around 490 nm. Fan et al. (2021) discovered that each P fraction had a distinct reflectance spectrum, but total P had characteristic bands in the vicinity of different wavelengths, that is, 250, 300, 400, 560, 735, and 750 nm. Additionally, they stated that both qualitative and quantitative assessments of total P could be accomplished using the Vis and NIR spectral regions.

Spectroscopic methods are common proximal sensing tools that acquire spectrum samples from restricted areas. Despite not having explicit spatial information, they have a high spectral resolution. On the other hand, multispectral imaging mounted on unmanned aerial vehicles (UAV) allows collecting both detailed spectral and precise spatial information. Yet, multispectral imaging sensors cover a small number of bands of the spectrum compared to the hyperspectral imaging sensors. However, they are still an affordable solution due to their low economical operating cost (Adão et al. 2017). UAV multispectral imagery has been widely used in agriculture for biophysical measurements like biomass, leaf area index, height, and crop cover, and biochemical characteristics such as chlorophyll and nutrients' content (Xie and Yang 2020). Soil nutrients estimation using UAV multispectral imagery can be done using crop-based approach or soil-based approach. A crop-based approach, as an indirect mean for a soil fertility assessment, relies on the crop spectral information to detect soil nutrient content as the crop growth and development are highly impacted by soil nutrient status (Zhu et al. 2021). However, few studies investigated the relationship between canopy reflectance and soil phosphorus.

Bare soil-based approaches to predict phosphorus content were investigated using satellite imagery but no studies were conducted to estimate soil P using UAV imagery. Several spectral vegetation indices were found to be effective in predicting soil phosphorus using satellite imagery or spectroscopy techniques. The normalized difference vegetation index (NDVI), based on information from the red and near-infrared bands, was the most studied of these spectral indices, and it has been correlated to plant-available and total phosphorus (TP), through an indirect estimation (Misbah et al. 2022). NDVI had the best results compared to other studied indices for predicting TP and Olsen-P concentrations (Lin et al. 2015). NDVI derived from satellite imagery has been used to map variation in soil phosphorus for site-specific management by Gopp et al. (2019) and Mazur et al. (2022). In addition to NDVI, other spectral indices based on the red and NIR regions, that is, the transformed vegetation index (TVI), the simple ratio (SR) of NIR and red bands, and the green NDVI (GNDVI), were found to be the most important variables for predicting soil TP (Kim et al. 2014). In other study conducted by (Kawamura et al. 2011), phosphorus content in soils was predicted from plant P normalized difference vegetation indices based on the reflectance at 523 and 583 nm with an $R^2 = 0.89$. In addition to spectral features, Haralick texture indices are common descriptors of an image texture and surface roughness, and they can be

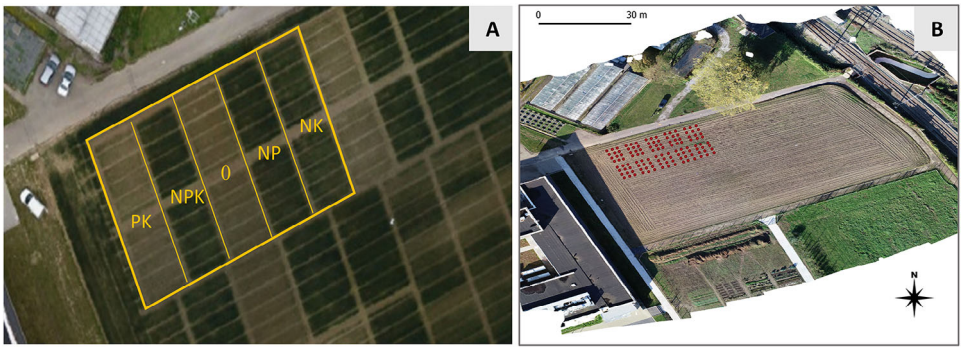

FIGURE 1 | Photos of the 100-year trial in Gembloux with the five fertilization treatments, each yellow rectangle represents a fertilization treatment divided into 10 microplots (A) the spatial distribution of the soil sampling points (B).

derived from remote sensed images. Haralick texture indices or texture information represent the spatial arrangement of pixel values in a pixel neighborhood (Kelsey and Neff 2014). As textural features provide very important spatial information of remotely sensed images, they have been widely combined with spectral information for predicting LAI (Zhou et al. 2022), crop yield, plant potassium accumulation, and/or characterizing plant diseases (Bebronne et al. 2020; Lu et al. 2021; Ma et al. 2022; Zhou et al. 2022). As such, they have been proven to improve the model's accuracy. To our knowledge, previously developed models for soil phosphorus prediction did not include Haralick textural features. Considering that available P fraction depends significantly on soil organic matter content, which itself has been demonstrated to be highly correlated to texture features (Roy et al. 2006), we presume that, in addition to the spectral data, texture features derived from bare soils before or after soil tillage can be important variables for soil phosphorus content prediction.

In this study, the effective spectral regions for detecting soil available and total P using visible and NIR spectroscopy were investigated. Subsequently, the acquisition was upgraded to UAV imagery to investigate the potential of combining spectral indices and texture features for predicting available and total P considering two different timings, that is, before and after seedbed preparation. The study provides a comprehensive analysis of soil P content using spatially explicit Vis-NIR data obtained from multispectral sensors mounted on UAV.

2 | Materials and Methods

2.1 | Experimental Site and Treatments

The study was conducted on a long-term trial located in Gembloux, Belgium (50°33′50.8″N, 4°41′55.7″E), called "the law of the minimum trial" (Figure 1A). The trial has been installed in 1896 to investigate the long-term effect of soil macronutrients' content, namely, nitrogen, phosphate, and potassium on crop yields and productivity. Considering the systematic fertilizers application and management, the trial consisted of five different rows; each row, 6 m wide, represents a different fertilization modality. Each row was divided into 10 microplots of 6 m long and 2 m wide (Figure 1B). Table 1 summarizes the treatments with the amount and timing of application. "NPK" stands for the fertilization treatment that supplies the three macronutrients (total nitrogen, phosphorus, and available potassium), "PK" stands for phosphopotassium fertilization, "NK" stands for nitrogen and potassium fertilization, "NP" stands for nitrogen and phosphorus fertilization, and "None" treatment stands for no application of the three macronutrients. The nutrients were applied during tillering stage (Z2.) according to Zadok scale for phosphorus, potassium, and the first fraction of the total amount of nitrogen. The second and the third applications of N were at Z30 and Z33 stages, respectively (Zadocks et al. 1974). The trial was supplied with the optimal rates of the essential nutrients, that is, K at 160 kg ha^{-1}, P at 120 kg ha^{-1}, and N at 150 kg ha^{-1} using potassium chloride, triple superphosphate, and ammonium nitrate fertilizers, respectively.

TABLE 1 | The applied treatments with the amounts of the macronutrients (N, P, and K) and their application time according to Zadocks scale.

	N			P2O5	K2O
Plots	**Z2.**	**Z30**	**Z39**	**Z21**	**Z21**
PK	—	—	—	120	160
NPK	50	50	50	120	160
0	—	—	—	—	—
NP	50	50	50	120	—
NK	50	50	50	—	160

2.2 | Soil Sampling and Spectra Measurement

Before carrying out UAV flights, soil samples were taken from a specific area within the 100-year trial, where the five fertilization treatments are located (PK, NPK, None, NP, and NK) as shown in Figure 1. Within this area, soil samples were collected from 120 points, a total of 24 soil samples were taken from each fertilization treatment, and the distance between 2 sampling points was 1.5 m. Samples were taken from the top 20 cm of the soil prior to tillage. Their exact location was georeferenced by a GNSS Leica ATX1230. The collected samples were subject to the following chemical analysis: nitrogen, potassium, AP, organic matter, pH, CEC, and TP. The plant-AP was determined according to Lakanen–Ervio method. This method extracts more P than the Olsen method but less P than the Mehlich 3 or Bray approaches, and it is routinely used in the Walloon region of Belgium (Renneson et al.

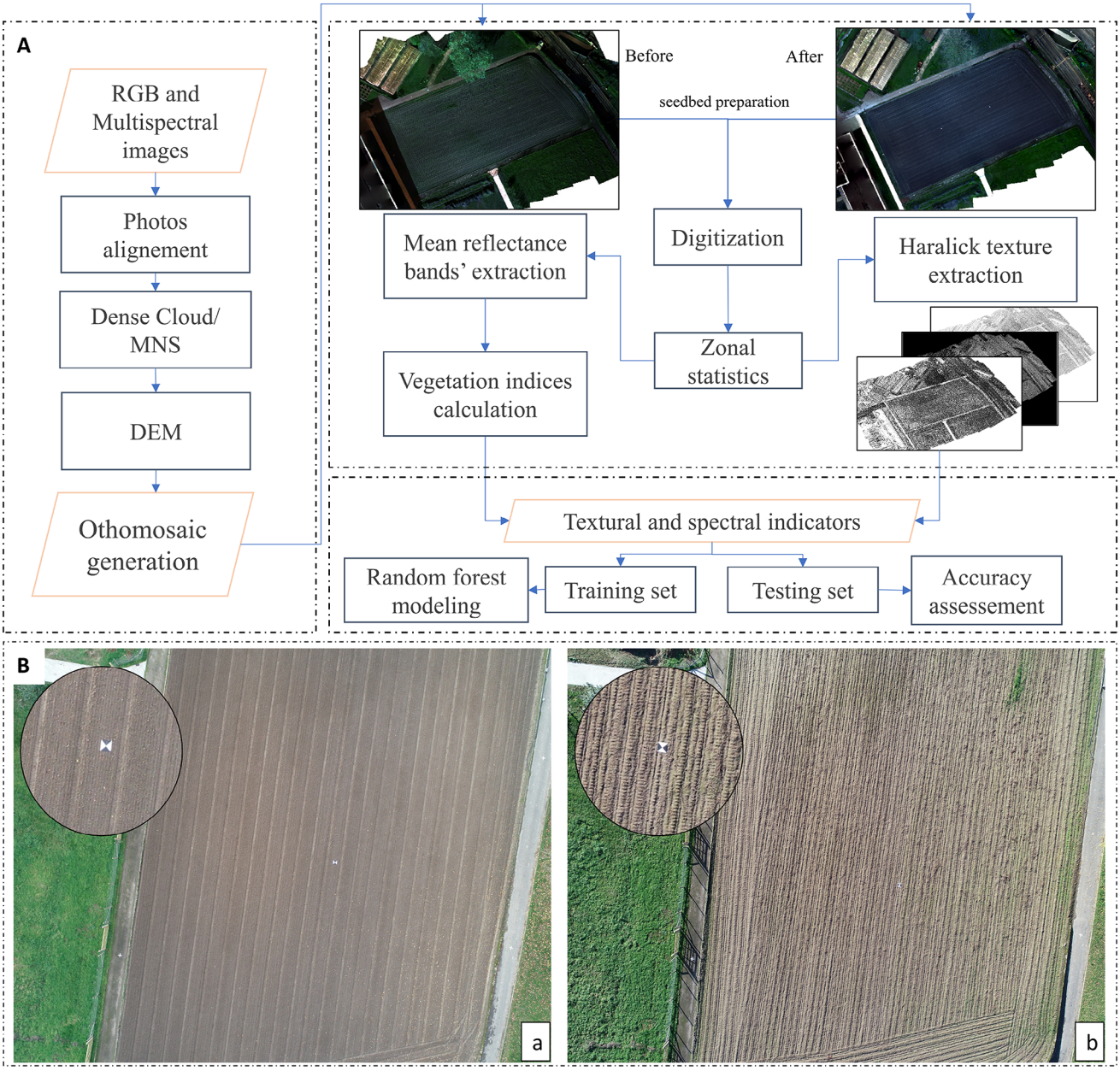

FIGURE 2 | Workflow of image processing, data extraction and modeling (A), RGB drone images of the trial before (B,a) and after seedbed preparation (B,b). DEM, digital elevation model.

2016). The methods for soil analysis of other soil properties (N, K, SOM, pH, CEC) are detailed in Table S1. The soil texture is silt loam according to Belgian soil texture classification triangle. The same dried and sieved samples, considering a 2 mm sieve, were subjected to spectral acquisition between 400 and 2500 nm using DS2500 Foss Vis-VIR spectrometer located at the Walloon Agricultural Research Centre (CRA-W). Reflectance data were computed as absorbances (log 1/R).

2.3 | Photogrammetric Data Acquisition

A first UAV flight was performed over the experimental site on November 5, 2020 prior to any tillage, and a second UAV flight was performed on November 26, 2020 after plowing, tilling soil to a depth of 20 cm, and seedbed preparation. A multirotor drone equipped with a Micasense Rededge multispectral camera (MicaSense, Seattle, WA, USA) and RGB camera was used. In total, 92 photos covered the whole area of the long-term trial (0.5 ha) during each flight. A total of 14 ground control points were recorded using precision GNSS Leica ATX1230. The Micasense Rededge has a focal length equal to 5.5 mm and a sensor size of $30 \times 30 \times 20$ mm^3, with a resolution of 1280×960 pixels. The RGB and multispectral cameras' respective ground sample distances (GSD) were 1.53 and 3.98 cm at 60 m flight altitude. The multispectral camera records five regions of the light spectrum: blue (B), green (G), red (R), red-edge (RE), and NIR with central bands and bandwidths of 475 ± 20, 560 ± 20, 668 ± 10, 717 ± 10, and 840 ± 40 nm, respectively (See Figure 2).

TABLE 2 | The list of the explanatory variables, their formulas, and their references.

Class	Variable	Formula	References
Spectral indices	NDVI	(NIR−R)/(NIR + R)	Rouse et al. (1974)
	GNDVI	(NIR−G)/(NIR + G)	Gitelson and Merzlyak (1998)
	NDRE	(NIR−RE)/(NIR + RE)	Gitelson and Merzlyak (1994)
	MSR	$(\mathrm{NIR/R}-1)/\sqrt{\mathrm{NIR}/R-1}$	Chen and Chen (1996)
	OSAVI	1.16[a](NIR—R)/(NIR + R + 0.16)	Rondeaux et al. (1996)
	RVI	NIR/R	Jordan (1969)
	SR	NIR/G	Tucker (1979)
	DVI	NIR—R	Becker and Choudhury (1988)
Textural indices	Energy	$\sum_{i=1}^{N}\sum_{j=1}^{N} p(i,j)^2$	Haralick et al. (1973)
	Entropy	$-\sum_{i=1}^{N}\sum_{j=1}^{N} p(i,j)\log p(i,j)$	
	Correlation	$\sum_{i=1}^{N}\sum_{j=1}^{N} \frac{(i.j)p(i,j)-\mu_x\mu_y}{\sigma_x\sigma_y}$	
	Homogeneity	$\sum_{i=1}^{N}\sum_{j=1}^{N} \frac{p(i,j)}{1+\lvert i-j\rvert}$	
	Inertia	$\sum_{i=1}^{N}\sum_{j=1}^{N} (i-j)^2 p(i,j)$	
	Cluster shade	$\sum_{i=1}^{N}\sum_{j=1}^{N} (i+j\lvert-2\mu)^4 p(i,j)$	
	Cluster prominenence	$\sum_{i=1}^{N}\sum_{j=1}^{N} (i+j\lvert-2\mu)^3 p(i,j)$	

Abbreviations: DVI, difference vegetation index; MSR, modified simple ratio; NDVI, normalized difference vegetation index; OSAVI, optimized soil adjusted vegetation index; RVI, vegetation ratio index; SR, simple ratio.

[a]The row and column numbers are represented by i and j, respectively. The value of the matrix at the associated row and column is represented by $x(i, j)$. $p(i, j)$ denotes the ratio of a matrix's value at a given row and column to the total of all its values. N stands for the matrix's length (width). The matrix's mean and variance in the directions x and y are represented by $(\mu x, \mu y)$ and $(\sigma x, \sigma y)$, respectively.

2.4 | Image Processing and Data Extraction

The 92 images were loaded in the software Agisoft Metashape (Agisoft LLC, St. Petersburg, Russia) to create an orthomosaic for each of the two acquisition dates (before and after tillage). First, the photos were aligned, and the 14 ground control points were loaded to generate an optimized sparse point cloud and a dense cloud afterwards. Second, the DEM (digital elevation model) was generated on the basis of all the points of the dense point cloud. Finally, ortho-rectification and image mosaic creation were carried out using the DEM. This orthomosaic combines separate photos that have been orthorectified, that is, edited to remove the influence of relief, shot angle, and lens aberrations. The final output of a mosaic image for each flight acquisition date was exported as a .tiff file. The images were read in QGIS software for spectral and textural features extraction (Figure 2).

Considering the plot size, 2 m × 6 m polygons were digitized and set as sample size. Zonal statistics were performed to calculate the mean reflectance values of all pixels within the plot polygon using QGIS. After extracting the mean reflectance values for each band, eight multispectral indices are calculated (Table 2). The vegetation indices are divided into SR indices like the vegetation ratio index (RVI) and SR, difference vegetation index (DVI), into normalized difference vegetation indices such as NDVI, green NDVI, and RE NDVI, and other spectral indices like the optimized soil adjusted vegetation index (OSAVI) and the modified simple ratio (MSR).

In addition to spectral indices, seven textural indices were calculated for each plot using the Haralick texture extraction method and the Orfeo toolbox in QGIS (Table 2). Haralick texture features are determined from the gray-level co-occurrence matrix (GLCM), a matrix that counts the co-occurrence of adjacent gray levels in the image (Haralick et al. 1973). Seven GLCM-based texture features were calculated from the red band, including Energy (texture uniformity), Entropy (measure of randomness of intensity image), Correlation (how correlated a pixel is to its neighborhood), Inverse Difference Moment (measures the texture homogeneity), Inertia (intensity contrast between a pixel and its neighborhood), Cluster Shade, and Cluster Prominence (characteristics of these textures indices are given in Table 2).

2.5 | Data Analysis and Modeling

2.5.1 | Partial Least Square Regression (PLSR)

The phosphorus content of 120 samples and their raw spectra were split randomly into a training set (n = 84, i.e., 70%) and testing set (n = 36, i.e., 30%). Using unprocessed spectra, the AP and TP prediction models using fivefold cross-validation and PLSR were developed in RStudio version 4.1 (RStudio Inc., Boston, MA, USA). The spectroscopic analysis was limited to the Vis-NIR regions (350–1100 nm) of the spectrum to compare the spectroscopy results with those of low-cost imaging sensors

that cover bands in the same regions. Four latent variables (LVs) were retained, explaining considerable variability with small errors. The models were validated in a second step, and the accuracy of the predictions was assessed using the coefficient of determination (R^2_v), the root mean square error ($RMSE_v$), and the ratio of performance to deviation ($RPIQ_v$). To determine the informative wavelengths used in building the PLS models, a variable selection was performed on the basis of the PLS regression coefficients of the first four LVs (Cai et al. 2008). The wavelengths with a high regression coefficient value are considered as the key wavelengths.

2.5.2 | Random Forest (RF)

After digitization and zonal statistics in QGIS, RF was performed on the spectral indices and texture features of the bare soil using Caret package in RStudio to predict soil AP and TP (Kuhn 2008). The number of observations was reduced to 40 because of the digitization process. For each microplot, the mean of the textural and spectral indices was computed over the whole plot, and the corresponding phosphorus content was calculated as the average of the three sampling points. The dataset was divided into a training set ($n = 28$, 70%) to perform the fivefold cross-validation and test set ($n = 12$, 30%) to test the models' accuracy. RF consists of generating a final prediction based on several decision trees built from bootstrapped datasets. Without using all variables at each node, the RF algorithm uses a random selection of the variables to find the optimum split criterion to build each single tree. In the RF model, two key parameters need to be tuned, that is, *mtry* and *ntree*, which signify the number of variables and the number of trees in the random subset at each split, respectively. Tuning these parameters showed that the model performed the best with a *mtry* value of 2 and *ntree* value of 500.

2.5.3 | Models' Accuracy Assessment

To assess the developed models' prediction accuracy, the coefficient of determination (R^2), the root mean square error (RMSE), and the ratio of performance to interquartile range (RPIQ) using the following expressions were calculated:

$$R^2 = 1 - \frac{\sum_i (yi - \hat{y}i)^2}{\sum_i (yi - \hat{y}i)^2}$$

$$\text{RMSE}\sqrt{\frac{\sum_i (yi - \hat{y}i)^2}{n}}$$

$$\text{RPIQ} = \frac{\text{IQ}}{\text{RMSE}}$$

where $\hat{y}$ is the predicted value of y, $\bar{y}$ is the mean values of y, n is the number of samples, SD refers to standard deviation, and i refers to the ith observation. IQ is the difference between the third quartile (Q3) and the first quartile (Q1) of the samples. A larger RPIQ value indicates improved model performance.

3 | Results

3.1 | Soil Nutrients Content

Boxplots comparing the soil macronutrients content in the plots fertilized by the five fertilization treatments (NK, None, NP, NPK, and PK) are given in Figure 3. Despite the small area of the experimental site, it showed high variability in soil phosphorus data. The TP content of the 120 collected samples ranges from 740 to 1150 mg kg^{-1}, whereas the available form of P content ranges from 40 to 140 mg kg^{-1}. The fraction of available P represents a small percentage of the TP, that is, between 5% and 12%. Moreover, the phosphorus, nitrogen, and potassium were correlated to other soil properties using Pearson correlation, and results are presented as scatter plots matrix (Figure S1). The AP and TP levels were strongly correlated, and both were positively associated with K and CEC, whereas they were poorly correlated to SOM and other soil properties.

3.2 | Vis-NIR Point-Based Analysis

3.2.1 | Soil Absorbance Spectra

Figure 4A displays the raw spectra for the 120 soil samples (A) and the average spectral signatures for the 5 fertilization treatments (Figure 4B). All spectral signatures exhibited the typical shape of soil absorbance from the visible to the SWIR region with high values in visible that decrease in NIR and SWIR and a series of local absorbance peaks due to water absorption bands (in the vicinity of 1400, 1900, and 2200 nm). In addition to the O–H bonds, the absorbance around 1400 and 1900 nm was also linked to aliphatic C–H and amide N–H, respectively. The comparison between the average spectral response of the five fertilization treatments shows overlapping spectra in the visible region with a distinctive difference in the NIR and SWIR regions. The lowest absorbance values were recorded for the NK treatment, whereas the non-fertilizer treatment showed the highest spectral values.

3.2.2 | PLSR Model

PLSRs were performed on the absorbance spectra in the range of 350–1100 nm to predict the soil available and total P. Figure 5 displays the results of the calibration using the fivefold cross-validation method and the validation procedure on an independent set to test the accuracy of both models to predict AP and TP contents. The highest correlations were obtained for AP in both calibration and validation processes ($R^2_{cv} = 0.82$ and $R^2_v = 0.74$, respectively) compared to TP prediction model, which had coefficients of determination equal to 0.71 and 0.68 for cross-validation and validation, respectively. The ratio of performance to deviation (RPIQ) for the AP validation model was equal to 285. It was noticed that the AP prediction model slightly outperforms the TP prediction model.

The importance of individual wavelengths in the regression model was revealed by the regression coefficients per LV of the developed PLS models. Figure 6 presents the regression coefficients plots for the first four LV for the AP and TP models.

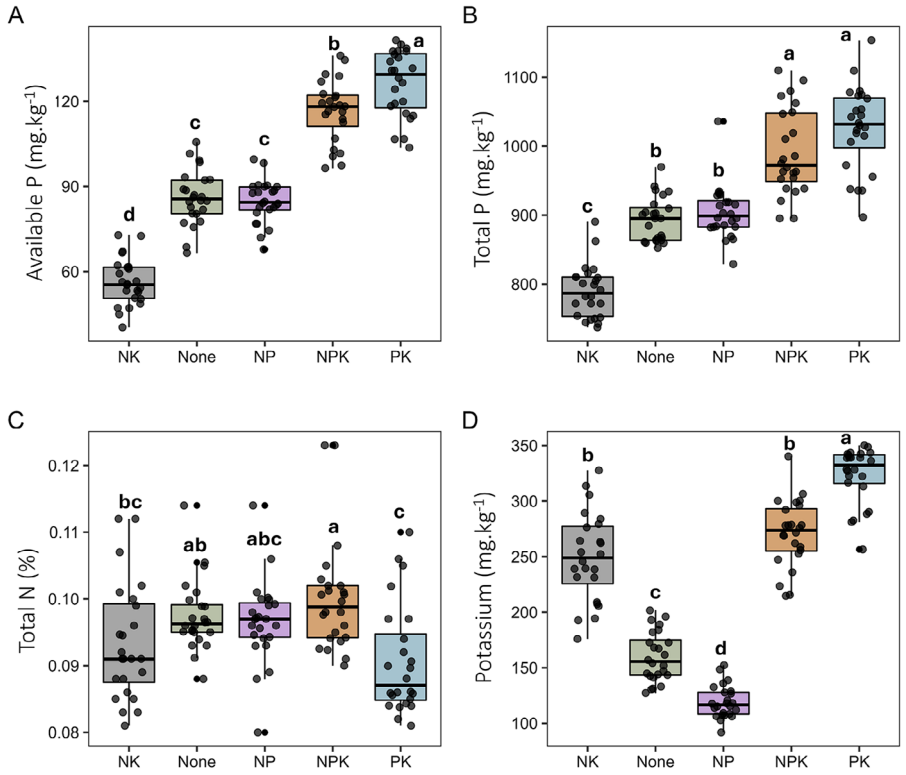

FIGURE 3 | Boxplots comparing available phosphorus (A), total phosphorus (B), total nitrogen (C), and potassium (D) for the studied fertilization modalities.

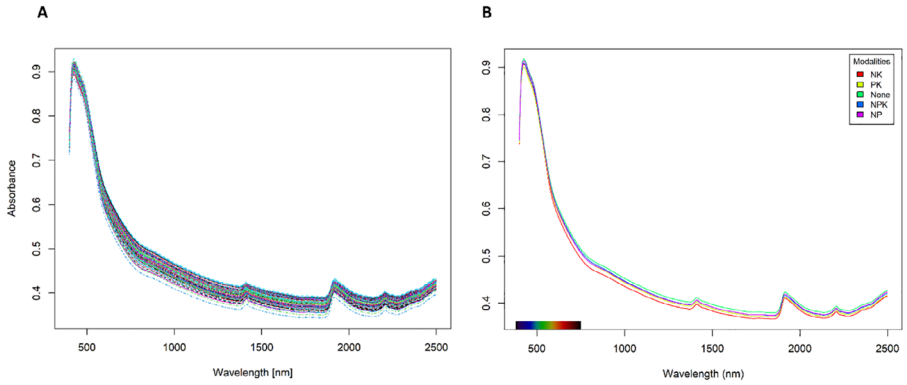

FIGURE 4 | The raw absorbance spectra (log 1/R) of soil collected samples from different fertilization modalities (A) and the average spectral signatures for the NK, PK, None, NPK, and NP treatments, each spectrum is an average of 24 samples (B).

The regression coefficients of soil phosphorus content in the PLS models indicate a high importance of wavelengths in the visible range. The variability in the spectra of both prediction models did not appear to be effectively explained by the first LV1. Nevertheless, the LV2 explained a small percentage of variation in the blue region around 450 nm, in addition to the LV3 and LV4 for both AP and TP prediction models. Looking at the regression coefficients for LV3 and LV4, it appears that LV3 and LV4 are strongly dependent on the spectral regions around 580 and 700 nm for establishing the AP prediction model (Figure 6A). In addition to these two peaks at 580 and 700 nm, TP is also dependent on wavelength 540 nm. We must point out that the wavelengths 540 and 580 nm correspond to the green band of the Micasense sensor, whereas the camera's RE is at 700 nm. The LV4 for both soil AP and TP had a regression coefficients peak at 850 nm in the NIR region. The peak was more relevant for TP than AP regression coefficients. The analysis was limited to the spectral range from 350 to 1100 nm; the calibration models for AP and TP, as well as the regression coefficient plots, can be found in the supplementary material (Figures S2 and S3).

3.3 | Remote Sensing and Prediction of P Content

3.3.1 | RF Model

The results of models' calibration and validation, for AP and TP before and after tillage, are presented in Figure 7. The models

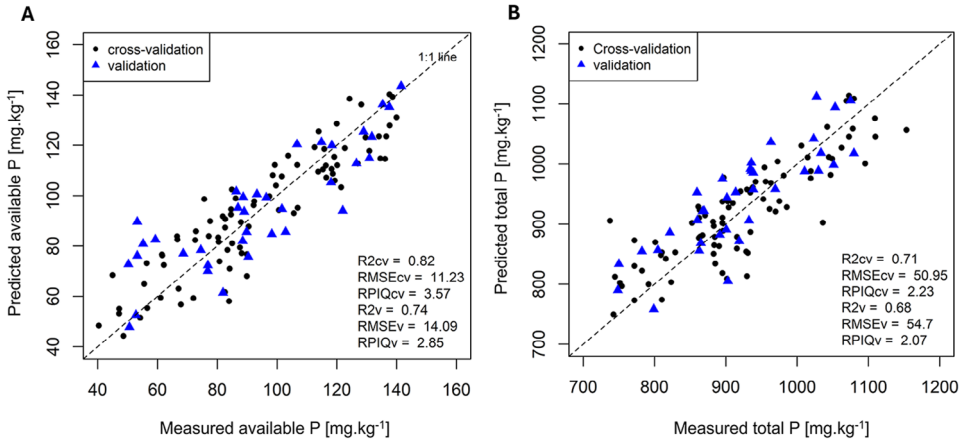

FIGURE 5 | Cross-validation and validation results of AP (A) and TP (B) PLS-based models. The calibration and test sets are presented by black filled circles and blue filled triangles, respectively.

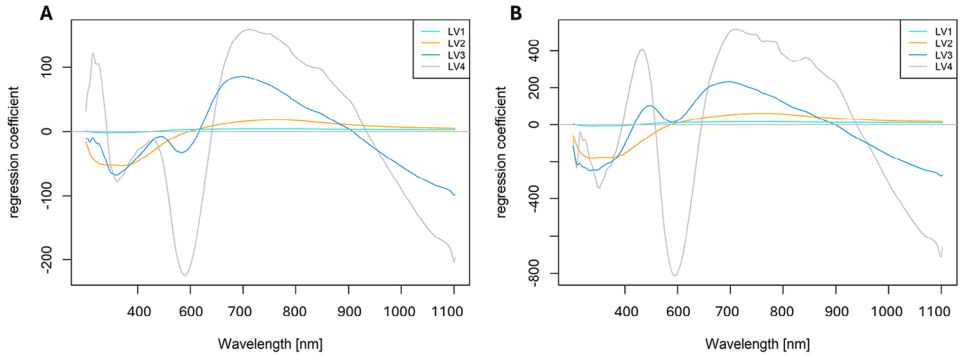

FIGURE 6 | Regression coefficients of PLS models for the prediction of available phosphorus content (A) and total phosphorus content (B). LV, latent variable.

produced various estimation accuracies for soil phosphorus. The model based on the before-tillage textural and spectral data to predict AP had R^2 values of 0.53 and 0.51 and RMSE values of 19.05 and 16.82 mg kg^{-1} for calibration and validation, respectively. After soil tillage, the AP model had a better performance in calibration (R^2_{cv} = 0.72 and $RMSE_{cv}$ = 20.43 mg kg^{-1}) and validation (R^2_v = 0.68, $RMSE_v$ = 13.65 mg kg^{-1}, and $RPIQ_v$ = 2.98) (Figure 7C). In contrast, the TP prediction model obtained before soil tillage was slightly better than the developed model after soil tillage with R^2_v = 0.49, $RMSE_v$ = 54.73 mg kg^{-1}, and $RPIQ_v$ = 2.06), but still not satisfactory (Figure 7B). Compared to the established models using the textural and spectral indices extracted from the before-tillage images, it appears that soil tillage decreased the accuracy of TP prediction model and increased soil AP estimation using spectral indices and textural indices.

3.3.2 | Variable Importance

Comparing before and after seedbed preparation, the relative importance of textural and spectral predictors in the developed RF models is presented in Figure 8. Before soil tillage, all the eight spectral indices were the most important variables in AP and TP prediction, which had relative importance greater than 60%. Textural features had relative importance inferior to 20% (Figure 8A,B). The first three spectral indices were NDRE, RVI, and MSR for AP prediction, whereas the multispectral indices NDRE, RVI, and GNDVI were the best predictors to explain the variability of soil TP before tillage. On the other hand, the single bands of red edge and red and textural indices were the most important variables for predicting soil AP and TP after soil tillage. When predicting AP, the relative importance values for the green band and the textural characteristics, inertia, and cluster prominence ranged from 60% to 80%. The remaining spectral bands and the textural features had relative importance values between 20% and 60% for both AP and TP prediction models. After soil tillage, the vegetation indices had low contributions in explaining the AP and TP soil variability, and hence, the relative importance values were inferior to 20% (Figure 8C,D). Results revealed that the vegetation indices explained variation of soil AP and TP before seedbed preparation, and textural indices became more important for estimating soil AP and TP after seedbed preparation.

4 | Discussion

In this study, the effect of soil phosphorus content on absorbance spectra was investigated to predict two phosphorus fractions, AP and TP, using visible and NIR spectroscopy. In our case, the AP fraction, determined using the Lakanen–Ervio method, ranges from 5% to 12% of TP. In similar conditions of 15-year

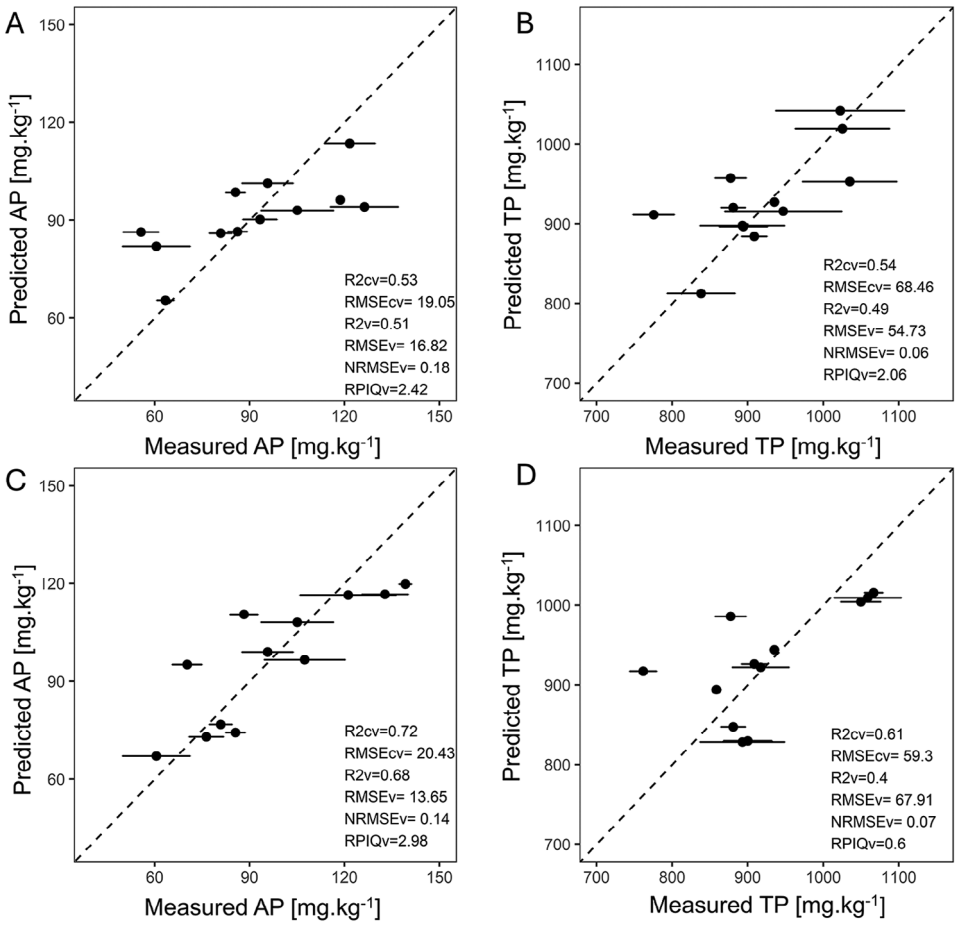

FIGURE 7 | The validation results of plant-available phosphorus (A and C) and total phosphorus (B and D) prediction models before tillage (A and B) and after tillage (C and D).

long-term fertilization trials, Olsen P represented 1%–13% of TP in all fertilization treatments, and the lowest values were recorded for the control treatment with no supply of macronutrients and the sole N fertilization (Shen et al. 2014). In our long-term trial, available P was lowest in the NK treatment, where no phosphorus was supplied. The results showed that this treatment exhibits the strongest decrease in absorbance in the NIR region. This decrease is more prominent in the NIR than in the visible region. Similarly, previous studies reported that decreasing P concentration decreases absorbance in the NIR and SWIR regions more than the visible region (Sridhar et al. 2009; Zhang and Zhang 2015).

Phosphorus and other nutrients cannot be directly predicted using spectroscopy, as they do not exhibit well-defined spectral responses. However, they can be indirectly detected when correlated with soil properties that have distinct spectral features (Niederberger et al. 2015; Reda et al. 2020). This indirect approach has led to variability in prediction results, with sensitive wavelengths reported in the visible, near-infrared, and shortwave infrared regions (Zhang and Zhang 2015). Here, the spectroscopic analysis was limited to the Vis-NIR regions (400–1100 nm) of the spectrum to compare the spectroscopy results with those of low-cost imaging sensors that cover bands in the same spectral regions. Narrowing down the spectral range to the visible and near-infrared region would prevent interference of soil P prediction wavelengths with other soil properties, like soil organic matter and soil moisture, as it was predominantly reported to absorb in the SWIR region (Viscarra Rossel et al. 2016).

In similar studies using the visible and near-infrared spectral range, the prediction of AP using raw spectra from 325 to 1075 nm yielded an R^2 of 0.69 and an RMSE of 5.76 mg kg^{-1}. The peaks at 460, 550, and 740 nm were found to be more significant for predicting AP (Xuemei and Jianshe 2013). Similarly, Jiang et al. (2023) found that the feature bands for AP were mostly concentrated around 500 and 700–1000 nm. When using the full spectrum from 450 to 2400 nm, AP was predicted with a validation R^2 of 0.79 and an RPIQ of 3.55 (Yu et al. 2023). However, they identified feature bands for AP between 400 and 1100 nm at 499, 516, 542, 745, and 770 nm. Singha et al. (2023) predicted AP with R^2 of 0.71 and RPIQ of 3.44 and reported sensitive wavelengths of 430 and 505 nm for AP. However, for predicting TP, Fan et al. (2021) found that the diagnostic spectrum of TP is distributed across the 250–750 nm range, with specific wavelengths at 250, 300, 400, 560, 735, and 750 nm. Using this range, the prediction model for TP achieved an R^2 of 0.87 and an RPD of 2.66. Consistent with our findings, peaks around 540, 580, and 700 nm, as well as in the NIR region around 850 nm, were found to be the most important wavelengths in predicting AP and TP. Models based on Vis-NIRS for predicting AP showed higher performances compared to TP prediction models (Abdi et al. 2016; Recena et al. 2019).

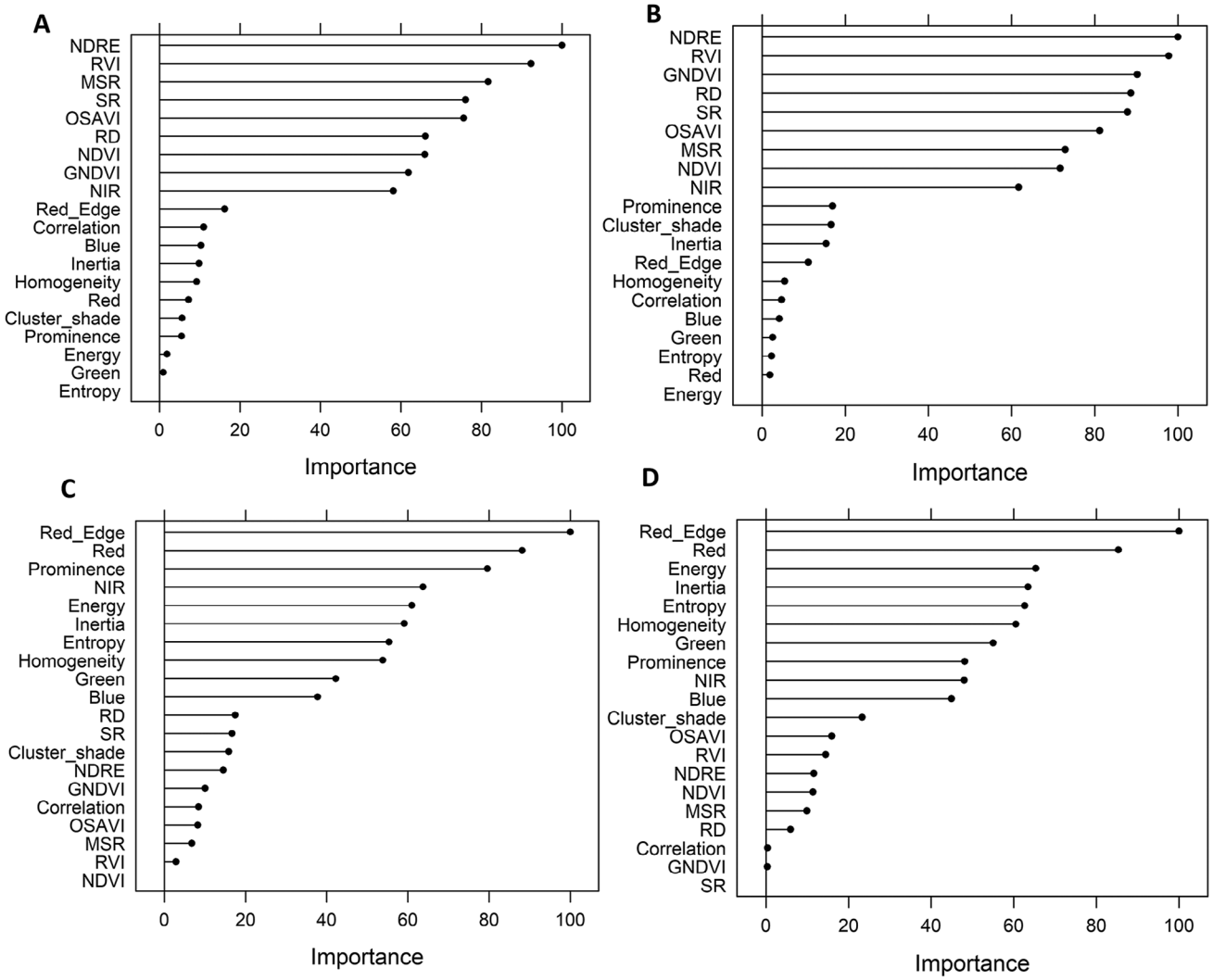

FIGURE 8 | Variable importance plots for plant-available phosphorus and total phosphorus RF prediction models before tillage (A and B, respectively) and after tillage (C and D). MSR, modified simple ratio; NDVI, normalized difference vegetation index; NIR, near infrared; OSAVI, optimized soil adjusted vegetation index; RVI, vegetation ratio index; SR, simple ratio.

In the second part of our research, the information derived from the Vis and NIR bands of low-cost imaging sensor mounted on a UAV was analyzed to determine whether the resulting data may be used for soil P prediction in field conditions. The models for predicting both AP and TP exhibited different performances before and after soil tillage, with improved accuracy observed post-tillage. This raises the question of how soil tillage affects phosphorus prediction accuracy. Soil tillage reduces aggregate which increases the amount of energy reflected, resulting in higher vegetation index values and greater reflectance in the red and NIR wavelengths (Sadeghi et al. 2018). Additionally, tillage and seedbed preparation can effectively reduce weed density and incorporate vegetation cover, contributing to a more homogeneous and smoother soil surface after tillage (Figure 1B).

Before soil tillage, the vegetation indices ranked high in the RF prediction models for AP and TP as compared to those developed after using tillage image-derived indices. As a result, we conclude that the information obtained from these images is primarily affected by the reflectance of vegetation cover, weeds, and stubbles that were present in the field prior to the seedbed preparation, which impacted the accuracy of phosphorus predictions (Figure 1B). Various soil features, including vegetation cover and crop residue, can affect the spectral response of remote sensing images, thus decreasing prediction accuracy (Biney et al. 2023; Pimstein et al. 2011). Variability in the distribution of vegetation cover may have led to high variability in vegetation index values before soil tillage, as bare soil and crop residue exhibit different spectral reflectance. The effect of fractional vegetation cover on spectral information and the accuracy of predicting soil properties has been studied by Bartholomeus et al. (2009), who reported that vegetation significantly affects soil properties prediction accuracy. Even with low amounts of fractional vegetation cover, predictions can become inaccurate, and the degree of inaccuracy depends on the fractional vegetation cover, the index used, and the specific soil property being measured. Yue et al. (2020) differentiated the fractional cover of vegetation, crop residue, and bare soil in cropland systems using the broadband crop residue angle index. For SOC, it was stated that the primary factor contributing to predictions inaccuracy and reliability was the presence of crop residue partially covering the soil surface (Dvorakova et al. 2020; Rodionov et al. 2014).

Among several vegetation indices, NDRE and RVI, R ranked high in the variable importance for the AP and TP models. Each of these indices uses the spectral wavelength bands (red and NIR) in its formulas. Lin et al. (2015) reported that TP and Olsen-P concentrations can be indirectly estimated using an optimized index in the red and near-infrared wavelengths (NDVI). The R^2 of validation set were approximately 0.48 and 0.5 for TP and Olsen-P, respectively. A correlation analysis was done by Mazur et al. (2022) where a significant positive relationship was observed between the NDVI and bare soil phosphorus content ($r = 0.61$). Kim et al. (2014) found also that the vegetation indices based on the red and NIR bands, TVI, SR, NDVI green, and NDVI are the most important variables of RF model for TP prediction.

After seedbed preparation, the single spectral bands RE, red, and green ranked high in variable importance of the RF model for AP prediction, which corresponds to the wavelengths with the highest regression coefficients in the PLS model generated using Vis and NIR spectra for soil AP. The texture features also ranked high in variable importance after seedbed preparation. However, the integration of textural indices in predicting soil phosphorus or soil nutrients content has not been taken into consideration in past studies. According to this research, soil tillage and seedbed preparation made an important contribution to the model's accuracy when predicting AP. In addition to incorporating vegetation cover and minimizing the effects of vegetation cover on spectral data and prediction accuracy, soil tillage and seedbed preparation alter soil roughness, resulting in a more homogeneous and smoother surface (Figure 1B). It has been reported that soil roughness is one of the major factors influencing the soil reflectance spectrum in the field (Angelopoulou et al. 2019). On rough soils, Rodionov et al. (2014) observed a significant overestimation of soil organic carbon content. However, the impact of soil roughness on soil nutrient prediction has not been extensively studied, especially at the field scale. In general, soil surface roughness influences the accuracy and the reliability of the predictions, and this factor must be considered during the preprocessing and interpretation of image data. Predicting quantitative surface soil properties relies on the availability of exposed bare soil, preferably under seedbed conditions, to minimize the influence of confounding factors such as vegetation cover, crop residues, and soil roughness (Herodowicz and Piekarczyk 2018). This has been confirmed by our study, which showed that soil tillage minimized the effect of vegetation cover and altered the impact of roughness, leading to higher accuracy in predicting soil phosphorus.

5 | Conclusion

Vis and NIR spectroscopy is a rapid and nondestructive technique for predicting various soil parameters. The raw spectra from Vis-NIR spectroscopy, in combination with PLS regression, proved effective in estimating available and TP (R^2_v = 0.74 and 0.68 and $RPIQ_v$ = 2.85 and 2.07 for AP and TP, respectively). With the purpose of detecting soil phosphorus across a larger scale within field conditions, we investigated the potential of UAV multispectral imagery to assess soil phosphorus. This involves using textural and spectral features derived from UAV multispectral imagery based on a relatively small number of samples imposed by the long-term experiment. We found that spectral indices combined with texture features predict plant-AP with a good accuracy after soil tillage (i.e., $R^2_v = 0.68$, $RMSE_v = 13.65$ mg kg^{-1}, and $RPIQ_v = 2.98$). For nonmobile nutrients, such as phosphorus, where the only accurate and realistic approach to determining crop needs is soil analysis before sowing, we consider that our findings are promising for predicting soil phosphorus using UAV imagery of bare soil. We conclude that soil phosphorus prediction using UAV imaging techniques is more accurate on a prepared seedbed as soil tillage and seedbed preparation can effectively reduce weed density and incorporate vegetation cover, contributing to a more homogeneous and smoother soil surface after tillage and more accurate prediction of soil P contents. However, the model should be calibrated for more campaigns under normal field conditions to get models that are robust to variation in soils conditions.

Acknowledgments

The authors would like to thank the Walloon Agricultural Research Centre (CRA-W) for the soil spectra acquisition. The authors are grateful to Francoise Thys and Jesse Jap for the field data collection.

Conflicts of Interest

The authors declare no conflicts of interest.

Data Availability Statement

The data that support the findings of this study are available from the corresponding author upon reasonable request.

References

Abdi, D., B. J. Cade-Menun, N. Ziadi, G. F. Tremblay, and L. É. Parent. 2016. "Visible Near Infrared Reflectance Spectroscopy to Predict Soil Phosphorus Pools in Chernozems of Saskatchewan." *Canada. Geoderma Regional* 7: 93–101. https://doi.org/10.1016/j.geodrs.2016.02.004.

Adão, T., J. Hruška, L. Pádua, et al. 2017. "Hyperspectral Imaging: A Review on UAV-Based Sensors, Data Processing and Applications for Agriculture and Forestry." *Remote Sensing* 9: 1110. https://doi.org/10.3390/rs9111110.

Angelopoulou, T., N. Tziolas, A. Balafoutis, G. Zalidis, and D. Bochtis. 2019. "Remote Sensing Techniques for Soil Organic Carbon Estimation: A Review." *Remote Sensing* 11: 1–18. https://doi.org/10.3390/rs11060676.

Bartholomeus, H. 2009. "The Influence of Vegetation Cover on the Spectroscopic Estimation of Soil Properties." Ph.D. Thesis, Wageningen University, Wageningen, The Netherlands.

Bebronne, R., A. Carlier, R. Meurs, et al. 2020. "In-field Proximal Sensing of *Septoria tritici* Blotch, Stripe Rust and Brown Rust in Winter Wheat by Means of Reflectance and Textural Features From Multispectral Imagery." *Biosystems Engineering* 197: 257–269. https://doi.org/10.1016/J.BIOSYSTEMSENG.2020.06.011.

Becker, F., and B. J. Choudhury. 1988. "Relative Sensitivity of Normalized Difference Vegetation Index (NDVI) and Microwave Polarization Difference Index (MPDI) for Vegetation and Desertification Monitoring." *Remote Sensing of Environment* 24: 297–311. https://doi.org/10.1016/0034-4257(88)90031-4.

Biney, J. K. M., J. Houška, J. Volánek, D. K. Abebrese, and J. Cervenka. 2023. "Examining the Influence of Bare Soil UAV Imagery Combined With Auxiliary Datasets to Estimate and Map Soil Organic Carbon Distribution in an Erosion-Prone Agricultural Field." *Science of the Total Environment* 870: 161973. https://doi.org/10.1016/j.scitotenv.2023.161973.

Bogrekci, I., and W. S. Lee. 2006. "Effects of Soil Moisture Content on Absorbance Spectra of Sandy Soils in Sensing Phosphorus Concentrations

Using Uv–Vis-Nir Spectroscopy." *Transactions of the ASABE* 49: 1175–1180. https://doi.org/10.13031/2013.21717.

Cai, W., Y. Li, and X. Shao. 2008. "A Variable Selection Method Based on Uninformative Variable Elimination for Multivariate Calibration of Near-Infrared Spectra." *Chemometrics and Intelligent Laboratory Systems* 90: 188–194. https://doi.org/10.1016/J.CHEMOLAB.2007.10.001.

Chen, J. M., and M. J. Chen. 1996. "Evaluation of Vegetation Indices and a Modified Simple Ratio for Boreal Applications." *Canadian Journal of Remote Sensing* 22: 229–242. https://doi.org/10.1080/07038992.1996.10855178.

Dvorakova, K., P. Shi, Q. Limbourg, and B. Van Wesemael. 2020. "Soil Organic Carbon Mapping From Remote Sensing: The Effect of Crop Residues." *Remote Sensing* 12: 1–25. https://doi.org/10.3390/rs12121913.

Fan, P., X. Li, H. Qiu, and G. L. Hou. 2021. "Spectral Analysis of Total Phosphorus in Soils Based on Its Diagnostic Reflectance Spectra." *Results in Chemistry* 3: 100145. https://doi.org/10.1016/J.RECHEM.2021.100145.

Gholizadeh, A., M. Soom, M. Saberioon, and S. Farming. 2013. "Visible and Near Infrared Reflectance Spectroscopy to Determine Chemical Properties of Paddy Soils." *Journal of Food, Agriculture and Environment* 11: 859–866.

Gitelson, A., and M. N. Merzlyak. 1994. "Spectral Reflectance Changes Associated With Autumn Senescence of *Aesculus hippocastanum* L. and *Acer platanoides* L. Leaves. Spectral Features and Relation to Chlorophyll Estimation." *Journal of Plant Physiology* 143: 286–292. https://doi.org/10.1016/S0176-1617(11)81633-0.

Gitelson, A. A., and M. N. Merzlyak. 1998. "Remote Sensing of Chlorophyll Concentration in Higher Plant Leaves." *Advances in Space Research* 22: 689–692. https://doi.org/10.1016/S0273-1177(97)01133-2.

Gopp, N. V., O. A. Savenkov, T. V. Nechaeva, N. V. Smirnova, and A. V. Smirnov. 2019. "Application of NDVI in Digital Mapping of Phosphorus Content in Soils and Phosphorus Supply Assessment in Plants." *Izvestiya, Atmospheric and Oceanic Physics* 55: 1322–1328. https://doi.org/10.1134/S0001433819090196.

Haralick, R. M., I. Dinstein, and K. Shanmugam. 1973. "Textural Features for Image Classification." *IEEE Transactions on Systems, Man, and Cybernetics* SMC-3: 610–621. https://doi.org/10.1109/TSMC.1973.4309314.

Herodowicz, K., and J. A. N. Piekarczyk. 2018. "Effects of Soil Surface Roughness on Soil Processes and Remote Sensing Data Interpretation and Its Measuring Techniques—A Review." *Polish Journal of Soil Science* 51: 229. https://doi.org/10.17951/PJSS.2018.51.2.229.

Hu, G., K. A. Sudduth, and D. He. 2016. "Soil Phosphorus and Potassium Estimation by Reflectance Spectroscopy." *Transactions of the ASABE* 59: 97–105. https://doi.org/10.13031/trans.59.11048.

Jiang, C., J. Zhao, and G. Li. 2023. "Integration of Vis—NIR Spectroscopy and Machine Learning Techniques to Predict Eight Soil Parameters in Alpine Regions." *Agronomy* 13: 11–2816. https://doi.org/10.3390/agronomy13112816.

Jordan, C. F. 1969. "Derivation of Leaf-Area Index From Quality of Light on the Forest Floor." *Ecology* 50: 663–666. https://doi.org/10.2307/1936256.

Kawamura, K., A. D. Mackay, M. P. Tuohy, K. Betteridge, I. D. Sanches, and Y. Inoue. 2011. "Potential for Spectral Indices to Remotely Sense Phosphorus and Potassium Content of Legume-Based Pasture as a Means of Assessing Soil Phosphorus and Potassium Fertility Status." *International Journal of Remote Sensing* 32: 103–124. https://doi.org/10.1080/01431160903439908.

Kawamura, K., Y. Tsujimoto, T. Nishigaki, et al. 2019. "Laboratory Visible and Near-Infrared Spectroscopy With Genetic Algorithm-Based Partial Least Squares Regression for Assessing the Soil Phosphorus Content of Upland and Lowland Rice Fields in Madagascar." *Remote Sensing* 11: 506. https://doi.org/10.3390/RS11050506.

Kelseyx, K., and J. Neff. 2014. "Estimates of aboveground biomass from texture analysis of landsat imagery." *Remote Sens.* 6: 6407–6422. https://doi.org/10.3390/rs6076407.

Kim, J., S. Grunwald, and R. G. Rivero. 2014. "Soil Phosphorus and Nitrogen Predictions Across Spatial Escalating Scales in an Aquatic Ecosystem Using Remote Sensing Images." *IEEE Transactions on Geoscience and Remote Sensing* 52: 6724–6737. https://doi.org/10.1109/TGRS.2014.2301443.

Kodaira, M., and S. Shibusawa. 2013. "Using a Mobile Real-Time Soil Visible-Near Infrared Sensor for High Resolution Soil Property Mapping." *Geoderma* 199: 64–79. https://doi.org/10.1016/j.geoderma.2012.09.007.

Kuang, B., H. S. Mahmood, M. Z. Quraishi, W. B. Hoogmoed, A. M. Mouazen, and E. J. van Henten. 2012. "Sensing Soil Properties in the Laboratory, In Situ, and on-Line: A Review." *Advances in Agronomy* 114: 155–223. https://doi.org/10.1016/B978-0-12-394275-3.00003-1.

Kuhn, M. 2008. "Building Predictive Models in R Using the Caret Package." *Journal of Statistical Software* 28: 1–26. https://doi.org/10.18637/jss.v028.i05.

Lin, C., R. Ma, Q. Zhu, and J. Li. 2015. "Using Hyper-Spectral Indices to Detect Soil Phosphorus Concentration for Various Land Use Patterns." *Journal of Statistical Software*, 28: 1–26. https://doi.org/10.1007/s10661-014-4130-x.

Lu, J., J. U. H. Eitel, M. Engels, et al. 2021. "Improving Unmanned Aerial Vehicle (UAV) Remote Sensing of Rice Plant Potassium Accumulation by Fusing Spectral and Textural Information." *International Journal of Applied Earth Observation and Geoinformation* 104: 102592. https://doi.org/10.1016/J.JAG.2021.102592.

Ma, Y., L. Ma, Q. Zhang, et al. 2022. "Cotton Yield Estimation Based on Vegetation Indices and Texture Features Derived from RGB Image." *Frontiers in Plant Science* 13: 1–17. https://doi.org/10.3389/fpls.2022.925986.

Madsen, E. L. 1995. "Impacts of Agricultural Practices on Subsurface Microbial Ecology." *Advances in Agronomy* 54: 1–67. https://doi.org/10.1016/S0065-2113(08)60897-4.

Maleki, M. R., A. M. Mouazen, H. Ramon, and J. De Baerdemaeker. 2007. "Optimisation of Soil VIS–NIR Sensor-Based Variable Rate Application System of Soil Phosphorus." *Soil and Tillage Research* 94: 239–250. https://doi.org/10.1016/J.STILL.2006.07.016.

Mazur, P., D. Gozdowski, and E. Wójcik-Gront. 2022. "Soil Electrical Conductivity and Satellite-Derived Vegetation Indices for Evaluation of Phosphorus, Potassium and Magnesium Content, pH, and Delineation of Within-Field Management Zones." *Agriculture* 12: 883. https://doi.org/10.3390/agriculture12060883.

Misbah, K., A. Laamrani, K. Khechba, D. Dhiba, and A. Chehbouni. 2022. "Multi-Sensors Remote Sensing Applications for Assessing, Monitoring, and Mapping NPK Content in Soil and Crops in African Agricultural Land." *Remote Sensing* 14: 81. https://doi.org/10.3390/rs14010081.

Niederberger, J., B. Todt, A. Boča, et al. 2015. "Use of Near-Infrared Spectroscopy to Assess Phosphorus Fractions of Different Plant Availability in Forest Soils." *Biogeosciences* 12: 3415–3428. https://doi.org/10.5194/BG-12-3415-2015.

Pätzold, S., M. Leenen, P. Frizen, T. Heggemann, P. Wagner, and A. Rodionov. 2019. "Predicting Plant Available Phosphorus Using Infrared Spectroscopy With Consideration for Future Mobile Sensing Applications in Precision Farming." *Precision Agriculture* 21: 737–761. https://doi.org/10.1007/s11119-019-09693-3.

Pimstein, A., G. Notesco, and E. Ben-Dor. 2011. "Performance of Three Identical Spectrometers in Retrieving Soil Reflectance Under Laboratory Conditions." *Soil Science Society of America Journal* 75: 746–759. https://doi.org/10.2136/SSSAJ2010.0174.

Recena, R., V. M. Fernández-Cabanás, and A. Delgado. 2019. "Soil Fertility Assessment by Vis-NIR Spectroscopy: Predicting Soil Functioning Rather Than Availability Indices." *Geoderma* 337: 368–374. https://doi.org/10.1016/J.GEODERMA.2018.09.049.

Reda, R., T. Saffaj, S. E. Itqiq, et al. 2020. "Predicting Soil Phosphorus and Studying the Effect of Texture on the Prediction Accuracy Using Machine Learning Combined With Near-Infrared Spectroscopy." *Spectrochimica Acta Part A Spectrochimica Acta, Part A: Molecular and Biomolecular Spectroscopy* 242: 118736. https://doi.org/10.1016/J.SAA.2020.118736.

Renneson, M., S. Barbieux, and G. Colinet. 2016. "B A Indicators of Phosphorus Status in Soils: Significance and Relevance for Crop Soils in Southern Belgium. A Review." *Biotechnology, Agronomy, Society and Environment* 20: 257–272.

Rodionov, A., S. Pätzold, G. Welp, R. C. Pallares, L. Damerow, and W. Amelung. 2014. "Sensing of Soil Organic Carbon Using Visible and Near-Infrared Spectroscopy at Variable Moisture and Surface Roughness." *Soil Science Society of America Journal* 78: 949–957. https://doi.org/10.2136/SSSAJ2013.07.0264.

Rondeaux, G., M. Steven, and F. Baret. 1996. "Optimization of Soil-Adjusted Vegetation Indices." *Remote Sensing of Environment* 55: 95–107. https://doi.org/10.1016/0034-4257(95)00186-7.

Rouse, J. W. J., R. H. Haas, J. A. Schell, et al. 1974. *Monitoring Vegetation Systems in the Great Plains With ERTS*. NASA. Goddard Space Flight Center 3d ERTS-1 Symposium, 1: 309–317.

Roy, S. K., S. Shibusawa, and T. Okayama. 2006. "Textural Analysis of Soil Images to Quantify and Characterize the Spatial Variation of Soil Properties Using a Real-Time Soil Sensor." *Precision Agriculture* 7: 419–436. https://doi.org/10.1007/s11119-006-9018-5.

Sadeghi, M., E. Babaeian, M. Tuller, and S. B. Jones. 2018. "Particle Size Effects on Soil Reflectance Explained by an Analytical Radiative Transfer Model." *Remote Sensing of Environment* 210: 375–386. https://doi.org/10.1016/J.RSE.2018.03.028.

Shen, P., X. h. He, M. G. Xu, et al. 2014. "Soil Organic Carbon Accumulation Increases Percentage of Soil Olsen-P to Total P at Two 15-Year Mono-Cropping Systems in Northern China." *Journal of Integrative Agriculture* 13: 597–603. https://doi.org/10.1016/S2095-3119(13)60717-0.

Singha, C., K. C. Swain, S. Sahoo, and A. Govind. 2023. "Prediction of Soil Nutrients Through PLSR and SVMR Models by VIs-NIR Reflectance Spectroscopy." *Egyptian Journal of Remote Sensing and Space Science* 26: 901–918. https://doi.org/10.1016/j.ejrs.2023.10.005.

Sridhar, B. B. M., R. K. Vincent, J. D. Witter, and A. L. Spongberg. 2009. "Mapping the Total Phosphorus Concentration of Biosolid Amended Surface Soils Using LANDSAT TM Data." *Science of the Total Environment* 407: 2894–2899. https://doi.org/10.1016/J.SCITOTENV.2009.01.021.

Stewart, J. W. B., and H. Tiessen. 1987. "Dynamics of Soil Organic Phosphorus." *Biogeochemistry* 4: 41–60. https://doi.org/10.1007/BF02187361.

Tucker, C. J. 1979. "Red and Photographic Infrared Linear Combinations for Monitoring Vegetation." *Remote Sensing of Environment* 8: 127–150. https://doi.org/10.1016/0034-4257(79)90013-0.

Viscarra Rossel, R. A., T. Behrens, E. Ben-Dor, et al. 2016. "A Global Spectral Library to Characterize the World's Soil." *Earth-Science Reviews* 155: 198–230. https://doi.org/10.1016/J.EARSCIREV.2016.01.012.

Wijewardane, N. K., Y. Ge, S. Wills, and Z. Libohova. 2018. "Predicting Physical and Chemical Properties of US Soils With a Mid-Infrared Reflectance Spectral Library." *Soil Science Society of America Journal* 82: 722–731. https://doi.org/10.2136/sssaj2017.10.0361.

Xie, C., and C. Yang. 2020. "A Review on Plant High-Throughput Phenotyping Traits Using UAV-Based Sensors." *Computers and Electronics in Agriculture* 178: 105731. https://doi.org/10.1016/j.compag.2020.105731.

Xuemei, L., and L. Jianshe. 2013. "Measurement of Soil Properties Using Visible and Short Wave-Near Infrared Spectroscopy and Multivariate Calibration." *Measurement* 46: 3808–3814. https://doi.org/10.1016/j.measurement.2013.07.007.

Yu, B., C. Yan, J. Yuan, N. Ding, and Z. Chen. 2023. "Prediction of Soil Properties Based on Characteristic Wavelengths With Optimal Spectral Resolution by Using Vis-NIR Spectroscopy." *Spectrochimica Acta, Part A: Molecular and Biomolecular Spectroscopy* 293: 122452. https://doi.org/10.1016/j.saa.2023.122452.

Yue, J., Q. Tian, X. Dong, and N. Xu. 2020. "Using Broadband Crop Residue Angle Index to Estimate the Fractional Cover of Vegetation, Crop Residue, and Bare Soil in Cropland Systems." *Remote Sensing of Environment* 237: 111538. https://doi.org/10.1016/j.rse.2019.111538.

Zadocks, J. C., T. T. Chang, and C. F. Konzak. 1974. "A Decimal Code for the Growth Stages of Cereals." *Weed Research* 14: 415–421. https://doi.org/10.1111/J.1365-3180.1974.TB01084.X.

Zhang, L., and R. Zhang. 2015. "Fast Detection of Inorganic Phosphorus Fractions and Their Phosphorus Contents." *Soil Based on Near-Infrared Spectroscopy* 46: 1405–1410. https://doi.org/10.3303/CET1546235.

Zhang, Y., A. Biswas, W. Ji, and V. I. Adamchuk. 2017. "Depth-Specific Prediction of Soil Properties In Situ Using Vis-NIR Spectroscopy." *Soil Science Society of America Journal* 81: 993–1004. https://doi.org/10.2136/SSSAJ2016.08.0253.

Zhou, C., Y. Gong, S. Fang, and K. Yang. 2022. "Combining Spectral and Wavelet Texture Features for Unmanned Aerial Vehicles Remote Estimation of Rice Leaf Area Index." *Front. Plant Sci*. 13: 957870. https://doi.org/10.3389/fpls.2022.957870.

Zhu, J., A. Wu, and G. Zhou. 2021. "Spatial Distribution Patterns of Soil Total Phosphorus Influenced by Climatic Factors in China's Forest Ecosystems." *Scientific Reports* 11: 5357. https://doi.org/10.1038/s41598-021-84166-0.

Zhu, W., E. E. Rezaei, H. Nouri, et al. 2021. "Quick Detection of Field-Scale Soil Comprehensive Attributes via the Integration of UAV and Sentinel-2B Remote Sensing Data." *Remote Sensing* 13: 4716. https://doi.org/10.3390/rs13224716.

Supporting Information

Additional supporting information can be found online in the Supporting Information section.